INTERNATIONAL JOURNAL FOR NUMERICAL METHODS IN FLUIDS, VOL. 18, 215–226 (1994)

A NEW GENERAL-PURPOSE LEAST-SQUARES FINITE ELEMENT MODEL FOR STEADY INCOMPRESSIBLE LOW-VISCOSITY LAMINAR FLOW USING ISOPARAMETRIC C^1-CONTINUOUS HERMITE ELEMENTS

V. NASSEHI AND J. PETERA

Department of Chemical Engineering, Loughborough University of Technology, Loughborough, Leics LE11 3TU, U.K.

SUMMARY

This paper deals with a critical evaluation of various finite element models for low-viscosity laminar incompressible flow in geometrically complex domains. These models use Galerkin weighted residuals UVP, continuous penalty, discrete penalty and least-squares procedures. The model evaluations are based on the use of appropriate tensor product Lagrange and simplex quadratic triangular elements and a newly developed isoparametric Hermite element. All of the described models produce very accurate results for horizontal flows. In vertical flow domains, however, two different cases can be recognized. Downward flows, i.e. when the gravitational force is in the direction of the flow, usually do not present any special problem. In contrast, laminar flow of low-viscosity Newtonian fluids where the gravitational force is acting in the direction opposite to the flow presents a difficult case. We show that only by using the least-squares method in conjunction with C^1-continuous Hermite elements can this type of laminar flow be modelled accurately. The problem of smooth isoparametric mapping of C^1 Hermite elements, which is necessary in dealing with geometrically complicated domains, is tackled by means of an auxiliary optimization procedure. We conclude that the least-squares method in combination with isoparametric Hermite elements offers a new general-purpose modelling technique which can accurately simulate all types of low-viscosity incompressible laminar flow in complex domains.

KEY WORDS Galerkin method Hermite, Lagrange and simplex finite elements Mixed UVP Continuous and discrete penalty Least-squares method Low-viscosity laminar flow

INTRODUCTION

From an experimental point of view, low-viscosity laminar flow is often difficult to generate and maintain. This type of flow, however, occurs during membrane filtration of slurries and in metal casting and thus its study is needed. In this paper we aim to show that despite the apparent simplicity of this type of flow, which can generally be considered as Newtonian, the numerical modelling of it is not a trivial task. In particular, when the flow has a vertical upward direction and the fluid viscosity is small enough to make the opposing gravitational force significant, it is very difficult to obtain accurate solutions. This is similar to the findings of other investigators concerned with the numerical modelling of buoyancy-driven flows and the upward flow of low-viscosity fluids in moving boundary problems such as metal-casting processes. These workers have made remarks about the lack of a general-purpose foolproof method in dealing with such flow situations.[1] In some cases they have devised *ad hoc* methods to deal with the gravitational force in the dynamical equations.[2]

0271–2091/94/020215–12$11.00

Received January 1993
Revised September 1993

The low-viscosity laminar flows considered in this work are not creeping Stokesian regimes and therefore a valid mathematical model for them should include the convection terms in the governing equations of motion. The resulting non-linearity precludes any analytical solution of the model even for cases where the flow domain geometry and boundary conditions are very simple. For a long axisymmetric pipe, however, the exit velocity profile can be considered as developed and numerically obtained solutions for this section can be compared directly with the analytical velocities. We present a test case where we can compare the numerically simulated exit velocity profiles and the flow domain pressure field with the analytical exit velocity and hydrostatic pressures. These comparisons are used to evaluate the accuracy of various scheme–element combinations which produce stable results for the flow regime under study. The inclusion of thermal effects does not alter the conclusions of this work and thus we consider isothermal laminar flows.

MATHEMATICAL MODEL

The steady isothermal flow of an incompressible Newtonian fluid is governed by the following equations of continuity and motion:

$$f_1 = \nabla \cdot \mathbf{v} = 0, \tag{1}$$

$$f_2 = \rho \mathbf{v} \cdot \nabla \mathbf{v} - \nabla \cdot \boldsymbol{T} - \mathbf{g} = 0, \tag{2}$$

where $\mathbf{v}$ is the velocity vector, ρ is the density, $\boldsymbol{T}$ is the total stress tensor and $\mathbf{g}$ is the body force vector. The total stress $\boldsymbol{T}$ is given by

$$\boldsymbol{T} = -p\boldsymbol{\delta} + \boldsymbol{\tau}, \tag{3}$$

where p is the pressure $\boldsymbol{\delta}$ is the unit second-order tensor and $\boldsymbol{\tau}$ represents the deviatoric stress. For a Newtonian fluid the deviatoric stress is expressed as

$$\boldsymbol{\tau} = 2\eta\boldsymbol{\Delta}, \tag{4}$$

where η is the Newtonian viscosity and $\boldsymbol{\Delta}$ is the rate-of-deformation tensor given as

$$\boldsymbol{\Delta} = \tfrac{1}{2}(\nabla \mathbf{v} + \nabla \mathbf{v}^T). \tag{5}$$

Weighted residual statement of the model equations

The prime unknowns in the model equations are replaced by approximate trial function representations $\tilde{\mathbf{v}}$ and $\tilde{\boldsymbol{T}}$ and the resulting residuals are weighted and integrated over the solution domain Ω to yield[3]

$$\int_\Omega w \nabla \cdot \tilde{\mathbf{v}} \, d\Omega = 0, \qquad \int_\Omega w(\rho \tilde{\mathbf{v}} \cdot \nabla \tilde{\mathbf{v}} - \nabla \cdot \tilde{\boldsymbol{T}} - \mathbf{g}) \, d\Omega = 0, \tag{6}$$

where w is an appropriate weight function. The trial functions are expressed in terms of basis functions N_j and cardinal co-ordinates as

$$\tilde{\mathbf{v}} = \sum N_j v_j, \tag{7}$$

$$\tilde{T} = \sum N_j T_j. \tag{8}$$

In the finite element context the interpolation functions will represent the basis functions and the

nodal values of the variables will be the cardinal co-ordinates. For simplicity of writing we drop the '$\sim$' sign in the following equations. Application of Green's theorem (integration by parts) to the stress term in equation (6) gives

$$\int_\Omega w\rho\mathbf{v}\cdot\nabla\mathbf{v}\,d\Omega + \int_\Omega \nabla w\cdot\boldsymbol{T}\,d\Omega - \int_\Gamma w\boldsymbol{T}\cdot\mathbf{n}\,d\Gamma - \int_\Omega w\mathbf{g}\,d\Omega = 0, \tag{9}$$

where Γ is the boundary surrounding Ω and $\boldsymbol{n}$ is the unit outward vector normal to Γ. Substituting for $\boldsymbol{T}$ in the second term of equation (9) from equation (3) gives

$$\int_\Omega w\rho\mathbf{v}\cdot\nabla\mathbf{v}\,d\Omega + \int_\Omega \nabla w\cdot\tau\,d\Omega - \int_\Omega \nabla w\cdot\delta p\,d\Omega - \int_\Omega w\mathbf{g}\,d\Omega = \int_\Gamma w\boldsymbol{T}\cdot\mathbf{n}\,d\Gamma. \tag{10}$$

We use the prescribed inlet velocity profiles together with the no-slip solid wall and stress-free exit conditions as the boundary data in the present study. Thus the general form of the boundary conditions used is

$$\mathbf{v} = \mathbf{v}_0 \quad \text{on } \Gamma_1 \text{ (inlet)}, \qquad \boldsymbol{T}\cdot\mathbf{n} = 0 \quad \text{on } \Gamma_2 \text{ (exit } \wedge \textit{ line of symmetry)},$$

$$v_1 = v_2 = 0 \quad \text{on } \Gamma_3 \text{ (walls)},$$

where

$$\Gamma_1 \cup \Gamma_2 \cup \Gamma_3 = \Gamma.$$

In the standard Galerkin method used here the weight and interpolation functions are identical.

Least-squares statement of the model equations

Replacing the prime unknowns in the model equations with the approximate representations in terms of trial functions, we obtain residuals. We then square and integrate these residuals over the solution domain to develop a functional statement as

$$G[(\tilde{\mathbf{v}}), \tilde{p}] = \int_\Omega [(\text{res } f_{2i})_i^2 + k(\text{res } f_1)^2]\,d\Omega, \tag{11}$$

where the index i refers to individual components of the tensorial variables with summation over the repeated index. The constant k is used to make the above statement dimensionally consistent. Minimization of the functional (11) leads to the working equations of the least-squares scheme.[4]

Finite element schemes

The Galerkin weighted residual methods used are as follows.

Mixed UVP formulation. In this scheme the working equations are based exactly on equations (6) and (10). The only important factor to consider is that for an incompressible flow the selected element discretization should be such that the BBL condition is satisfied.[5] Thus we have used isoparametric Taylor–Hood and Crouzeix–Raviart C^0-continuous elements of tensor product or quadratic triangular simplex type[6] in this scheme.

Continuous penalty formulation. In this scheme the pressure in the working equation (10) is replaced by

$$p = -\lambda\nabla\cdot\mathbf{v}, \tag{12}$$

where λ is a penalty parameter.[3] This results in a compact formulation in terms of the velocity components and the pressure should be calculated after obtaining the velocity field via variational recovery.[7] We have used isoparametric C^0-continuous quadrilateral and triangular elements in this formulation with a selectively reduced integration procedure where the penalty terms are evaluated with a higher degree of approximation.

Discrete penalty formulation. In this scheme the penalty equation (12) is initially discretized and then, using this discretized form, the pressure is eliminated from the set of working equations.[6] This again results in a compact formulation and the pressure is calculated separately using the solution obtained for the velocity field. This approach can most conveniently be adopted if the type of elements used allows a discrete elemental mass matrix inversion during the process of elimination of the pressure from the equations. Therefore we used C^0-continuous isoparametric Crouzeix–Raviart-type elements in this scheme.

Least-squares formulation. Using the finite element discretization, we develop the working equations of this scheme in terms of the nodal values of the variables and the associated interpolation functions in the r–z co-ordinate system. These working equations are expressed as

$$\begin{aligned}
\frac{\partial G}{\partial v_{rj}} &= \int_\Omega 2\left[f_{2r}\left(\rho \mathbf{v} \cdot \nabla N_j - \eta \Delta N_j + \frac{\eta N_j}{r^2} \right) + k f_1 \left(N_{j,r} + \frac{1}{r} N_j \right) \right] \mathrm{d}\Omega = 0, \\
\frac{\partial G}{\partial v_{zj}} &= \int_\Omega 2[f_{2z}(\rho \mathbf{v} \cdot \nabla N_j - \eta \Delta N_j) + k f_1 N_{j,z}] \, \mathrm{d}\Omega = 0, \\
\frac{\partial G}{\partial p_j} &= \int_\Omega 2(f_{2r} N_{j,r} + f_{2z} N_{j,z}) \, \mathrm{d}\Omega = 0,
\end{aligned} \tag{13}$$

where

$$\Delta = \frac{\partial^2}{\partial r^2} + \frac{1}{r}\frac{\partial}{\partial r} + \frac{\partial^2}{\partial z^2} \tag{14}$$

is the Laplacian in the cylindrical co-ordinate system and the measure of integration is given by

$$\mathrm{d}\Omega = r \, \mathrm{d}r \, \mathrm{d}z.$$

The set of equations (13) comprises the basic working equations in this scheme. The existence of second-order derivatives in these equations makes it necessary to use C^1-continuous elements in the least-squares formulation. Complications associated with the use of C^1 elements have been considered as a drawback for this scheme in the past.[8] In this paper we present a method for the development of isoparametric C^1-continuous Hermite elements which cope with the continuity requirement of the least-squares scheme as well as being very effective in dealing with domains with curved boundaries.

Four-node isoparametric C^1-continuous Hermite element

The basic procedure for the development of the Hermite elements used in this work consists of the following steps.

(i) A topological equivalent of the real domain using square elements is constructed in which the number of elements and nodes and the element connectivity remain the same as in the

solution domain. We define a local co-ordinate system ξ–η within each square element. We refer to these elements and their local co-ordinate system as the master elements and master co-ordinates respectively.

(ii) We construct an intermediate stage of mapping based on bilinear isoparametric shape functions between the master elements and the solution domain as if the latter is comprised of C^0 quadrilateral elements. This mapping is expressed as

$$\tilde{x} = \sum_I \tilde{N}_I \tilde{X}_I, \qquad \tilde{y} = \sum_I \tilde{N}_I \tilde{Y}_I, \tag{15}$$

where $\tilde{N}_I$ are the bilinear shape functions and $\tilde{X}_I$ and $\tilde{Y}_I$ are the nodal co-ordinates in a global co-ordinate system defining the intermediate stage of mapping (Figure 1). The purpose of this stage is to establish a one-to-one relation between the master and solution domains. It must be noted, however, that this mapping is continuous but not sufficiently smooth. Later in this section we show that the construction of isoparametric C^1 elements requires smoothness as well as continuity.

(iii) For the four-node elements chosen here there are four degrees of freedom per node. These degrees of freedom represent a given function V, the first derivatives of the function with respect to ξ and η and the second-order mixed derivative of the function. Therefore altogether we need to construct 16 interpolation functions to define the element. The 16 bicubic interpolation functions associated with a four-node rectangular Hermite element in a local co-ordinate system ξ and η are easily obtained via the tensor products of one-dimensional Hermite interpolation relations in terms of single variables.[9] Therefore within such an element a function $V(\xi, \eta)$ can be found as an interpolant given by

$$V(\xi, \eta) = \hat{\mathbf{N}}^{\mathrm{T}}(\xi, \eta) \cdot \mathbf{V}_{(l)}. \tag{16}$$

Here $\boldsymbol{V}_{(l)}$ is the nodel degree of freedom vector and $\hat{\mathbf{N}}(\xi, \eta)$ are the tensor product interpolation functions defined as

$$\hat{\mathbf{N}}(\xi, \eta) = \hat{\mathbf{M}}(\xi) \odot \hat{\mathbf{M}}(\eta) \tag{17}$$

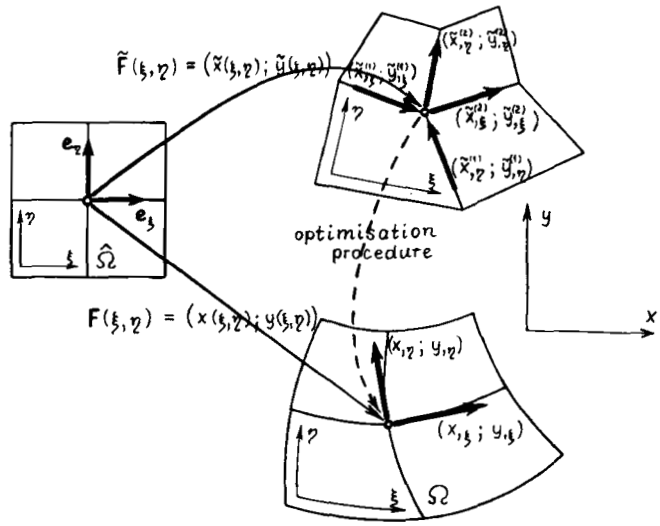

Figure 1. Construction of C^1 isoparametric mapping in curved domains

where $\hat{\mathbf{M}}(\xi)$ and $\hat{\mathbf{M}}(\eta)$ are one-dimensional Hermite shape functions. The 16 shape functions described above are represented as

$$\hat{\mathbf{N}} = [N_{Ii},\ I = 1, \ldots, 4,\ i = 1, \ldots, 4], \tag{18}$$

where I is the index for node numbers and i is the index for degrees of freedom. These shape functions fulfil the necessary requirements of linear independence.[10]

(iv) The final stage of construction of the isoparametric C^1 mapping is based on the definition of interpolation relations given by

$$x = \sum_I \sum_i \hat{N}_{Ii} X_{Ii}, \qquad y = \sum_I \sum_i \hat{N}_{Ii} Y_{Ii}, \tag{19}$$

where $\hat{N}_{Ii}$ ($I = 1, \ldots, 4$, $i = 1, \ldots, 4$) represent the previously constructed Hermite shape functions, x and y are the global co-ordinates in the real domain (Figure 1) and X_{Ii} and Y_{Ii} are the nodal degrees of freedom with respect to the global co-ordinate system. These are defined by

$$\mathbf{X}^{\mathrm{T}} = [\ldots; x_I; x_{,\xi j}; x_{,\eta I}; x_{,\xi\eta I}; \ldots], \qquad \mathbf{Y}^{\mathrm{T}} = [\ldots; y_I; y_{,\xi I}; y_{,\eta I}; y_{,\xi\eta I}; \ldots]. \tag{20}$$

Equations (19) involve C^1 Hermite shape functions and therefore describe a smooth mapping, but so far it is uncertain whether they give a one-to-one relation between the master and global domains. Since such a relation has already been given in terms of bilinear elements, it is evident that by minimizing the difference between these two mappings we may achieve this goal. This is done by an optimization process based on minimization of the functional

$$H(\mathbf{X}, \mathbf{Y}) = \tfrac{1}{2} \iint_{\hat{\Omega}} [(x - \tilde{x})^2 + (x_{,\xi} - \tilde{x}_{,\xi})^2 + (x_{,\eta} - \tilde{x}_{,\eta})^2 + (x_{,\xi\eta} - \tilde{x}_{,\xi\eta})^2 + (y - \tilde{y})^2 + (y_{,\xi} - \tilde{y}_{,\xi})^2 + (y_{,\eta} - \tilde{y}_{,\eta})^2 + (y_{,\xi\eta} - \tilde{y}_{,\xi\eta})^2]\, \mathrm{d}\xi\, \mathrm{d}\eta. \tag{21}$$

This leads to the construction of a set of linear algebraic equations in terms of the nodal values of geometrical functions and their derivatives (i.e. $\boldsymbol{X}$ and $\boldsymbol{Y}$). After insertion of the properly defined co-ordinates and derivatives at the external boundary nodes, this set becomes determinate and its solution provides nodal values at the internal grid points. At the external nodes the geometrical function values are found by the mollifier relation[10]

$$X_{Ii,k} = \int_{\hat{\Omega}} \hat{N}_{I1} \tilde{x}_{i,k}\, \mathrm{d}\xi\, \mathrm{d}\eta \Big/ \int_{\hat{\Omega}} \hat{N}_{I1}\, \mathrm{d}\xi\, \mathrm{d}\eta. \tag{22}$$

The use of these boundary values ensures that the obtained geometrical functions define a mapping image which closely represents the computational domain.

(v) The described isoparametric mapping gives relations between the master and real computational domains. These can be written as

$$x = x(\xi, \eta), \qquad y = y(\xi, \eta). \tag{23}$$

The corresponding shape (interpolation) functions are defined as

$$\mathbf{N}^{\mathrm{T}}(x, y) = \hat{\mathbf{N}}^{\mathrm{T}}(\xi(x, y); \eta(x, y)) \cdot \boldsymbol{C}, \tag{24}$$

where $\xi(x, y)$ and $\eta(x, y)$ are the inverse of the mapping relations given by (23) and $\boldsymbol{C}$ is expressed as

$$C = \begin{bmatrix} 1 & & & & & & 0 & \\ & x_{,\xi}^{(1)} y_{,\xi}^{(1)} & & & & & & \\ & x_{,\eta}^{(1)} y_{,\eta}^{(1)} & & & & & & \\ & & 1 & & & & & \\ & & & 1 & & & & \\ & & & & x_{,\xi}^{(2)} y_{,\xi}^{(2)} & & & \\ & & & & x_{,\eta}^{(2)} y_{,\eta}^{(2)} & & & \\ & 0 & & & & & 1 & \\ & & & & & & & \ddots \end{bmatrix} \tag{25}$$

which results from the construction of relations between the first-derivative degrees of freedom in the master and global co-ordinate systems. There is no need to relate the local and global values of mixed derivative degrees of freedom, because these derivatives are never given as boundary conditions. The solution of the model equations can be effectively carried out by maintaining these degrees of freedom at the local level. In other words, in any given problem the values of the function $V(x, y)$, the first derivatives $V_{,x}(x, y)$ and $V_{,y}(x, y)$ and the mixed derivative of the type $V_{,\xi\eta}(x, y)$ at the nodal points are sought as the necessary solution.

The first-order derivatives of the shape functions with respect to the global co-ordinates are given as

$$N_{,x}^{\mathrm{T}} = [\xi_{,x}\eta_{,x}] \begin{Bmatrix} \hat{\mathbf{N}}_{,\xi}^{\mathrm{T}} \\ \hat{\mathbf{N}}_{,\eta}^{\mathrm{T}} \end{Bmatrix} C, \tag{26}$$

$$N_{,y}^{\mathrm{T}} = [\xi_{,y}\eta_{,y}] \begin{Bmatrix} \hat{\mathbf{N}}_{,\xi}^{\mathrm{T}} \\ \hat{\mathbf{N}}_{,\eta}^{\mathrm{T}} \end{Bmatrix} C. \tag{27}$$

The C^1 continuity of the transformation implies that the inverse mapping is smooth and thus the derivatives of the shape functions with respect to the global co-ordinates are continuous. This in turn guarantees that the shape functions themselves are smooth. The second-order derivatives of the shape functions with respect to the global co-ordinates, which are necessary for the least-squares formulation, are found using the chain rule and are given as

$$\begin{aligned} N_{,xx} &= \hat{N}_{,\xi\xi}(\xi_{,x})^2 + 2\hat{N}_{,\xi\eta}\xi_{,x}\eta_{,x} + \hat{N}_{,\eta\eta}(\eta_{,x})^2 + \hat{N}_{,\xi}\xi_{,xx} + \hat{N}_{,\eta}\eta_{,xx}, \\ N_{,xy} &= \hat{N}_{,\xi\xi}\xi_{,x}\xi_{,y} + \hat{N}_{,\xi\eta}(\xi_{,x}\eta_{,y} + \xi_{,y}\eta_{,x}) + \hat{N}_{,\eta\eta}\eta_{,x}\eta_{,y} + \hat{N}_{,\xi}\xi_{,xy} + \hat{N}_{,\eta}\eta_{,xy}, \\ N_{,yy} &= \hat{N}_{,\xi\xi}(\xi_{,y})^2 + 2\hat{N}_{,\xi\eta}\xi_{,y}\eta_{,y} + \hat{N}_{,\eta\eta}(\eta_{,y})^2 + \hat{N}_{,\xi}\xi_{,yy} + \hat{N}_{,\eta}\eta_{,yy}. \end{aligned} \tag{28}$$

Details of the derivation of the first- and second-order derivatives of the inverse transformation (i.e. ξ_x, ξ_{xx}, etc.) have been published previously.[11] The isoparametric Hermite shape functions described above are linearly independent since the transformation is one-to-one and they are smooth because the isoparametric mapping is smooth.

COMPUTATIONAL RESULTS AND DISCUSSION

Upward flow of water in a vertical pipe of 0·05 m diameter and 1 m length is chosen as the test problem. The boundary conditions in this problem are a given plug flow inlet velocity of 0·01 ms^{-1}, zero radial velocity at the exit and no-slip wall conditions. For the least-squares method, because of the use of Hermite elements, first-order derivatives of the velocity components

should also be specified. For the test problem the values of these derivatives on the domain boundaries are zero.

The prescribed zero radial velocity at the exit of this long pipe corresponds to a developed axial velocity profile at this section. This enables us to compare our computed exit velocities with the analytical results. We can also compare the numerically obtained pressure fields with the expected hydrostatic head for this problem. The Reynolds number for this flow is 500 and the convection terms in the governing equation of motion are significant, so the test problem

Table I. Comparison of simulated and analytically obtained exit velocities and of the calculated pressure drop with the hydrostatic pressure

		Mesh of 100 quadrilateral elements				Mesh of 200 triangular elements			
		Water $\eta = 10^{-3}$ Pa s		Higher viscosity $\eta = 1$ Pa s		Water $\eta = 10^{-3}$ Pa s		Higher viscosity $\eta = 1$ Pa s	
		Error (%)		Error (%)		Error (%)		Error (%)	
	Scheme	v_r, v_z	p	v_r, v_z	p	v_r, v_z	p	v_r, v_z	p
1	Continuous penalty bi-quadratic Lagrange elements; Mesh refined near the wall (standard Galerkin)	>50	1	1	1	>50	1	1	1
2	Continuous penalty bi-quadratic Lagrange elements; uniform mesh (standard Galerkin)	5	1	5	1	5	1	5	1
3	Discrete penalty bi-quadratic Crouziex–Raviart element with rotated three-node discontinuous pressure sampling; mesh refined near the wall (standard Galerkin)	1	5	1	5	—	—	—	—
4	Discrete penalty bi-quadratic Taylor–Hood element with four-node discontinuous pressure sampling; mesh refined near the wall (standard Galerkin)	5	1	5	1	—	—	—	—
5	UVP1 biquadratic Crouziex–Raviart element with rotated three-node discontinuous pressure sampling; mesh refined near the wall (standard Galerkin)	>50	1	5	1	—	—	—	—
6	UVP2 biquadratic Taylor–Hood element with four- or three-node continuous pressure sampling; mesh refined near the wall (standard Galerkin)	>50	>50	<0.2	<0.2	>50	>50	<0.2	<0.2
7	LSQ–isoparametric Hermite element; mesh refined near the wall	<0.2	<0.2	<0.2	<0.2	—	—	—	—

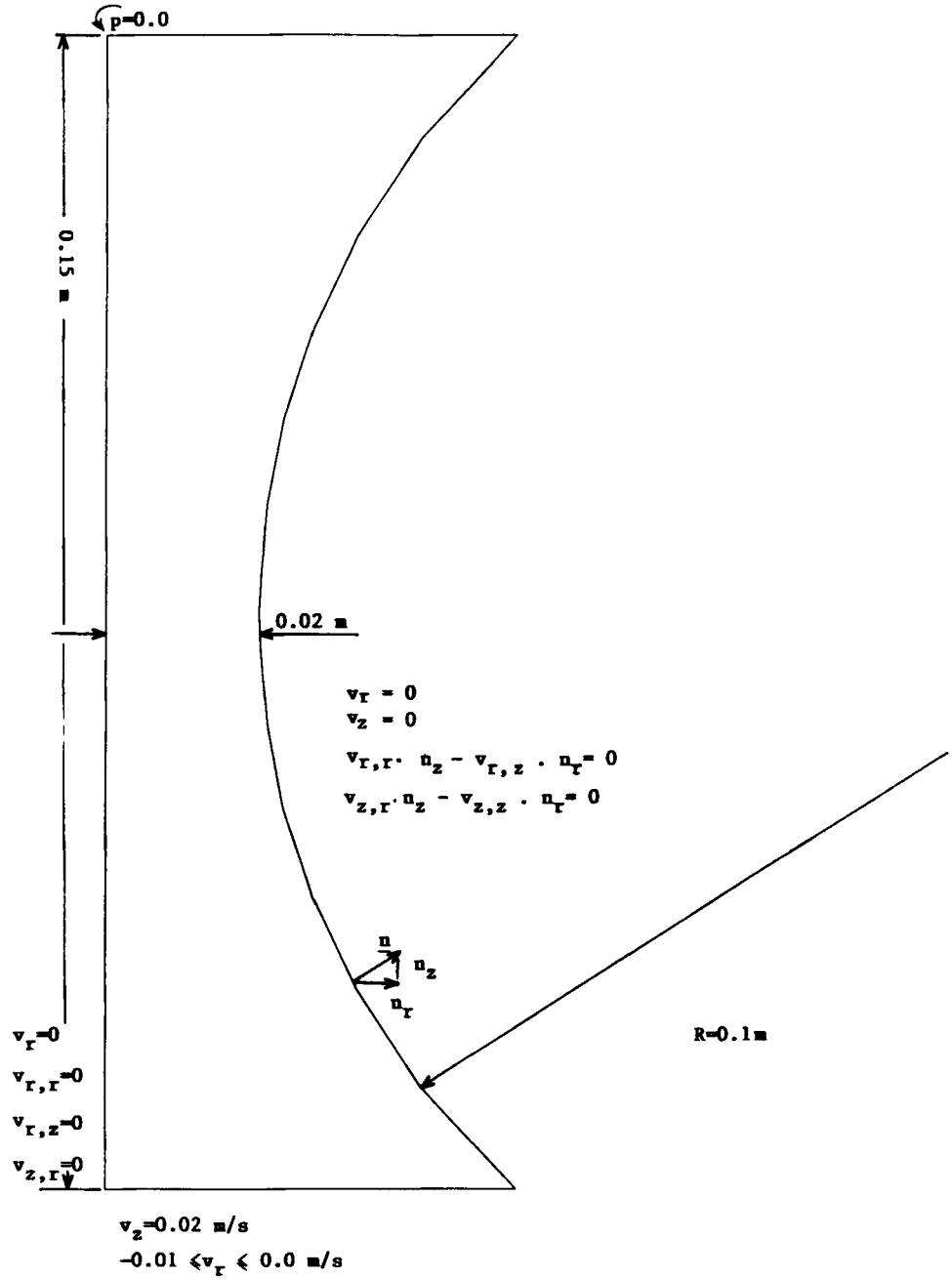

Figure 2. Flow domain dimensions and prescribed boundary conditions. Inlet velocities are chosen to be parallel to the element boundaries

represents a truly non-linear case. In order to show that the computational results are significantly affected by the fluid viscosity, we repeated the simulations for a similar flow regime with a higher viscosity of 1 Pa s.

Our conclusion is that except for the least-squares–Hermite element scheme, all methods fail to produce an acceptable velocity or pressure field for the vertical flow of water with opposing gravity. We found that as the fluid viscosity increases, the problem becomes easier and other schemes such as Galerkin weighted residual mixed UVP in conjunction with Taylor–Hood or triangular simplex elements also give very good results. This can be attributed to the fact that as the viscous forces in the equation of motion increase, the gravitational force becomes less significant. In Table I a summary of all our stable results for the test problem is given. The errors indicating the measure of accuracy of different scheme–element combinations are found on the basis of the previously described comparisons with analytical data. Except for the

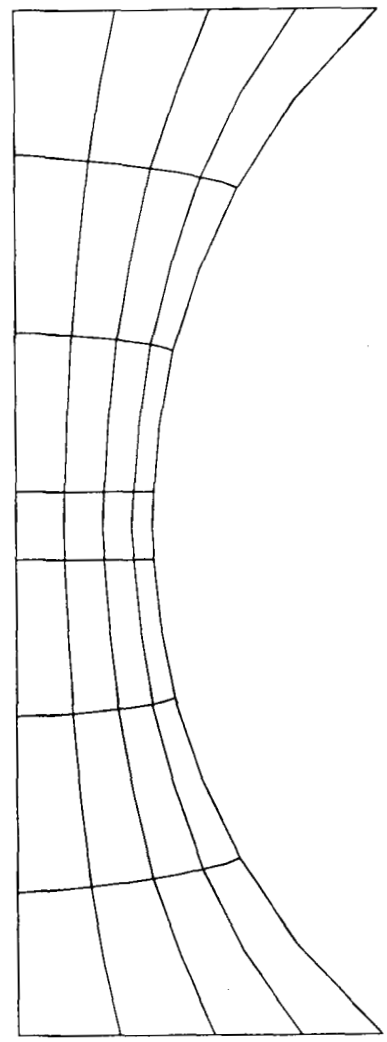

Figure 3. Coarse mesh of 28 four-node Hermite elements

least-squares method, all schemes produce much worse results (by as much as 20%) if only the near-solid-wall nodes are considered.

The dimensionality constant (k in equation (11)) in the least-squares method is found by trial and error. A value between 10^6 and 10^{10} is usually used. The best value for this constant in our test problem is 10^7. The use of such a large number makes the stiffness equation of the scheme ill-conditioned. In order to overcome this difficulty, we have applied a selectively reduced integration to evaluate terms multiplied by this constant. This is analogous to the treatment of the penalty parameter terms in the penalty methods. It can be shown, however, that while in the case of the penalty methods the use of selectively reduced integration is a must, for this situation it is only a preconditioning measure. Severely ill-conditioned stiffness matrices are encountered in all schemes which use the discontinuous three-node Crouziex–Raviart element. We found that a modification of the original element configuration based on 45° rotation of the

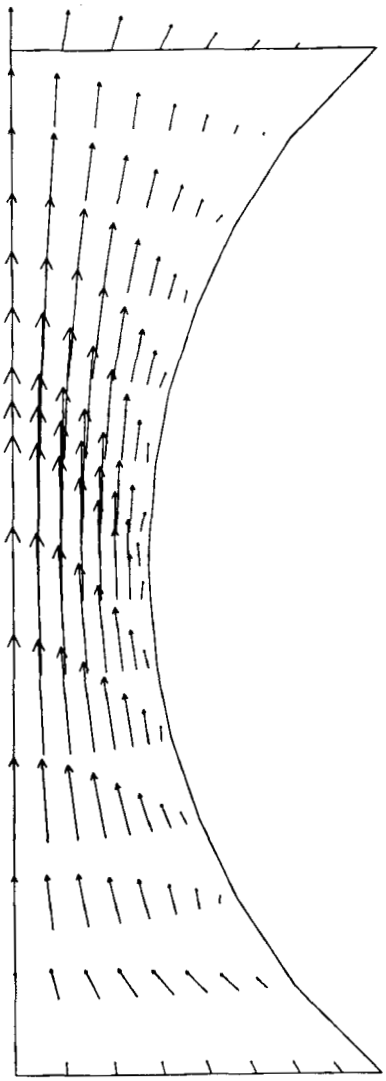

Figure 4(a) Computed velocity field

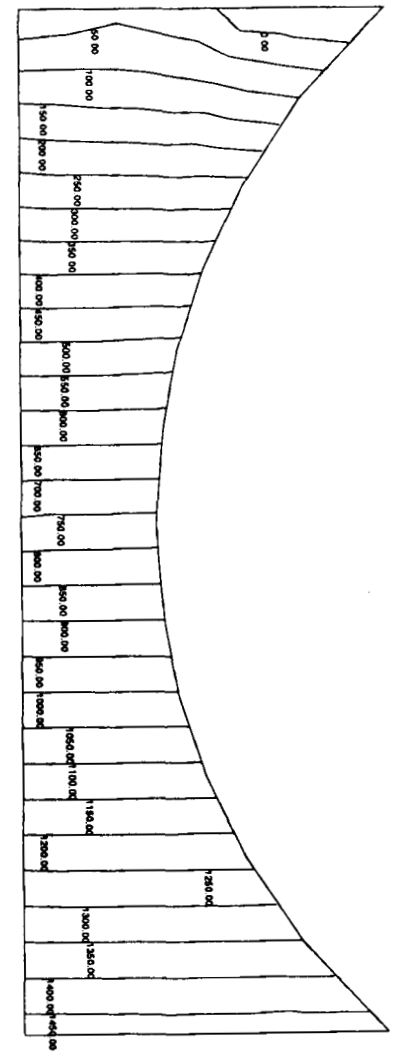

Figure 4(b) Computed pressure field

pressure-sampling nodes with respect to the local ξ η co-ordinate system resolves this difficulty. The described least-squares–isoparametric Hermite element scheme is a robust method and can deal with flow domains with curved boundaries. In order to illustrate this, we applied the model to simulate the vertical flow of water in a converging–diverging annulus with a given irregular inlet velocity profile. The isoparametric mapping of four-node Hermite elements even for a relatively coarse mesh with 28 distorted elements gives very reasonable results. The flow domain dimensions and prescribed boundary conditions are shown in Figure 2. In Figure 3 the finite element mesh used and in Figure 4(a) the corresponding computed velocity field are shown. In Figures 4(a) and 4(b) additional velocity and pressure values at centre nodes (which are not originally present in a four-node element discretization) are found by using interpolation procedures. The computed pressure isobars shown in Figure 4(b), except for an expected minor deviation at the exit section, correspond exactly to the hydrostatic pressure field representative of a low-viscosity vertical flow.

ACKNOWLEDGEMENT

The authors wish to express their gratitude to the Science and Engineering Research Council (U.K.) for a grant to support research work of which this study forms a part.

REFERENCES

1. D. H. Pelletier, J. N. Reddy and J. A. Scheltz, in C. L. Tien and T. C. Chawla (eds), *Annual Review of Numerical Fluid Mechanics and Heat Transfer*, Vol. II, Hemisphere, New York, 1989, Chap. 2.
2. B. D. Nichols, C. W. Hirt and R. S. Hotchkiss, 'Sola-Vof: a solution algorithm for transient fluid flow with multiple free boundaries', *Los Alamos Sci. Lab. Rep. LA-8355*, 1980.
3. T. J. R. Hughes, *The Finite Element Method*, Prentice-Hall, Englewood Cliffs, NJ, 1987.
4. O. C. Zienkiewicz, *The Finite Element Method*, McGraw-Hill, London, 1977.
5. J. N. Reddy, *Applied Functional Analysis and Variational Methods in Engineering*, McGraw-Hill, New York, 1986.
6. V. Girault and P. A. Raviart, *Springer Series SCM*, Vol. 5, *Finite Element Methods for Navier–Stokes Equations*, Springer, New York, 1986.
7. J. F. T. Pittman and S. Nakazawa, in J. F. T. Pittman, O. C. Zienkienicz, R. O. Wood and J. M. Alexander (eds), *Numerical Analysis of Forming Processes*, Wiley, New York, 1984, Chap. 6.
8. S. S. Rao, *The Finite Element Method in Engineering*, Pergamon, Oxford, 1982.
9. F. K. Bogner, R. L. Fox and L. A. Schmit, *Proc. Conf. on Matrix Methods in Structural Mechanics*, Wright Patterson AFB, Ohio, 1965.
10. J. T. Oden and J. N. Reddy, *An Introduction to the Mathematical Theory of Finite Elements*, Wiley, New York, 1976.
11. J. Petera, V. Nassehi and J. F. T. Pittman, 'Petrov-Galerkin methods on isoparametric bilinear and biquadratic elements: tested for a scalar convection–diffusion problem', *Int. J. Numer. Methods Heat Fluid Flow*, **3**, 205–221 (1993).